Volume 18, Number 5, 2025. pp. 561-571

Jordan Journal of Physics

ARTICLE

Exploring Strongly Correlated Rare-Earth Intermetallics: Theoretical Insights into RIn_3 and RSn_3 (R = Sm, Eu, Gd)

Aman Kumar[a] and **Anuj Kumar**[b]

[a] *Department of Physics, Faculty of Science, Swami Vivekanand Subharti University, Meerut, Uttar Pradesh, India.*

[b] *Department of Physics, Mahamaya Government Degree College, Sherkot, Bijnore, India.*

Doi: **https://doi.org/10.47011/18.5.1**

Received on: 23/11/2023; *Accepted on: 13/03/2025*

Abstract: The structural, electronic, magnetic, and elastic properties of Rin_3 and RSn_3 (R = Sm, Eu, Gd) were thoroughly investigated using the full potential linearized augmented plane wave plus local orbital (FP-LAPW+lo) method within the framework of density functional theory (DFT). Structural properties were evaluated using the local density approximation (LDA), generalized gradient approximation (GGA), and their band-correlated extensions, LDA+U and GGA+U. The computed lattice parameters exhibited excellent agreement with experimental results, and the divalent state of Eu was confirmed. To accurately predict the electronic properties, spin-orbit coupling (SOC) was incorporated, along with the splitting of the 4f states in rare-earth elements. Elastic properties, including bulk modulus, shear modulus, Young's modulus, anisotropic ratio, Kleinman parameters, Poisson's ratio, Lamé coefficients, sound velocities for shear and longitudinal waves, and Debye temperature, were calculated. Additionally, the Cauchy pressure and the B/G ratio were analyzed to determine the ductile or brittle nature of these compounds.

Keywords: Electronic properties, LDA+U, GGA+U, Elastic properties.

Introduction

Rare-earth elements, particularly those of the lanthanide series, are distinguished by their incomplete 4f electron shell, with unpaired electrons in the 4f subshell playing a pivotal role in determining their physical properties and those of their compounds [1-2]. Rare-earth intermetallic compounds have drawn substantial attention due to their unique properties, such as high melting points, excellent high-temperature ductility, superior mechanical strength, and advantageous electrical and magnetic characteristics. These attributes render them highly suitable for applications in the automotive, aviation, and aerospace industries. Additionally, rare-earth intermetallics outperform other metals by offering enhanced strength and stiffness, low specific weight, and excellent corrosion resistance, making them ideal for the development of commercial aviation turbines [3]. Approximately 90% of intermetallic compounds exhibit ductility due to the lack of d electrons near the Fermi level [4]. The intermetallic complexes RIn_3 and RSn_3 (R = rare-earth element) demonstrate intriguing properties arising from their incomplete 4f shell. These properties include diverse magnetic topologies, transitions between magnetic and non-magnetic states, valence fluctuations, and the formation of magnetic moments [5, 6]. Furthermore, RSn_3 intermetallic compounds have been identified as effective substitutes for lead, enhancing the efficiency of lead-free solder materials [7]. Rare-earth intermetallic compounds Rin_3 and RSn_3 (R = Sm, Eu, Gd) exhibit several remarkable properties [8, 9]. They adopt a cubic $AuCu_3$-type crystal structure within the space group *Pm-3m* (No. 221). In this structure, rare-earth atoms (R) occupy the 1a (0,

Corresponding Author: Aman Kumar **Email**: amankumar@gmail.com

0, 0) position, while non-magnetic elements like In and Sn are situated in the 3c position at (0, 1/2, 1/2). Most RIn_3 and RSn_3 compounds exhibit antiferromagnetic (AFM) ordering below 45 K [10-12]. Among the light rare-earth elements, the stability of Rin_3 and RSn_3 phases decreases from La to Gd [13]. Magnetic studies and lattice constant measurements confirm the characteristic lanthanide contraction of rare-earth elements, with exceptions observed in Eu and Yb compounds, where the rare-earth ions are divalent [14]. Antiferromagnetic transitions in the RIn_3 series occur at Néel temperatures (T_n) of 16, 10, and 42 K for $SmIn_3$, $EuIn_3$, and $GdIn_3$, respectively [15-17]. Similarly, in the RSn_3 series, $SmSn_3$, $EuSn_3$, and $GdSn_3$ exhibit antiferromagnetic transitions at T_n values of 12, 36.5, and 16.5 K, respectively [18]. Buschow *et al.* [12] investigated the magnetic properties and lattice parameters of the RIn_3 lanthanide family. Magnetic susceptibility measurements confirm that most compounds in the RIn_3 series exhibit antiferromagnetic ordering at low temperatures. Sanchez *et al*. [18] evaluated the electrical and magnetic properties of RSn_3 compounds (R = La, Ce, Pr, Nd, Sm, Eu, Gd, Yb) using Mössbauer spectroscopy, revealing complex magnetic structures in europium and gadolinium compounds. The Fermi surface properties of RIn_3 and RSn_3 were explored by Onuki and Settai [19], while Asadabadi *et al*. computed structural properties, such as lattice parameters and bulk modulus for RSn_3 (R = Sm, Eu, Gd), using local density approximation (LDA), generalized gradient approximation (GGA), and GGA+spin-polarized methods within the WIEN2K framework. Endoh *et al*. [20-21] conducted ultrasonic experiments to determine the elastic constants and investigated the influence of crystalline electric fields on the elastic constants of SmX compounds (X = Pd, In, Sn, Tl, Pb). Additionally, the role of rare-earth elements in RIn_3 and RSn_3 and their effects on electric field gradients (EFG) were analyzed by Asadabadi *et al*. [8] using density functional theory (DFT). Elastic constants play a crucial role in determining a material's response to external forces. They define the strength, brittleness, or ductility, and hardness of materials, while also providing valuable insights into bonding characteristics, anisotropy, and structural stability [22]. This study investigates the structural, electronic, elastic, and mechanical properties of rare-earth compounds RIn_3 and RSn_3 (R = Sm, Eu, Gd) using the full-potential linearized augmented plane wave plus local orbitals (FP-LAPW+lo) method within the framework of density functional theory (DFT).

Notably, this research is groundbreaking as it presents, for the first time, a detailed analysis of the elastic, mechanical, and thermal properties of these compounds through ab initio calculations.

Theoretical Method

This study utilized density functional theory (DFT) calculations implemented in the WIEN2K code [23] and employed the full-potential linearized augmented plane wave plus local orbitals (FP-LAPW+LO) method [24]. Exchange-correlation effects were computed using the local density approximation (LDA) [25] and generalized gradient approximation (GGA) [26], incorporating spin polarization. Recognizing Sn, Eu, and Gd as strongly correlated systems with localized 4f electrons, we applied the LDA+U and GGA+U methodologies to accurately determine their electronic structures. The GGA+U approach, based on the Hubbard model, effectively addresses strongly correlated systems by incorporating an orbital-dependent potential for Coulomb and exchange interactions [27]. Additionally, spin-orbit coupling (SOC) was included as a relativistic correction.

The muffin-tin sphere radii were set to 2.50 atomic units for rare-earth elements, tin, and indium. The basis set expansion was performed using plane waves with a product RMT × Kmax = 7, where RMT represents the smallest atomic radius in the unit cell, and Kmax is the largest k-vector value in the plane wave expansion. The angular momentum for the valence wave functions within the muffin-tin spheres was expanded up to lMAX = 10, and the charge density in the interstitial region was extended using Fourier analysis with a maximum reciprocal lattice vector of Gmax = 12. A dense k-point mesh of 165 k-points in the irreducible wedge of the Brillouin zone was generated using a Monkhorst-Pack grid of 18 × 18 × 18 [28], ensuring high accuracy in elastic property calculations.

The elastic constants (C_{11}, C_{12}, and C_{44}) were computed using the IR-elastic program implemented within the WIEN2K framework [29]. These calculations employed the GGA [26]

with spin polarization for the precise determination of elastic properties. Results were obtained for both spin-polarized and non-spin-polarized cases, and comparisons were made. Details regarding the IR-elastic methodology can be found in Ref. [30].

The energy-based methodology [31], as implemented in the WIEN2K code [23], was used to calculate the elastic constants. By employing Voigt notation and leveraging the symmetry of the cubic crystal lattice, the number of independent elastic constants was reduced to three: C_{11}, C_{12}, and C_{44}. This approach ensures computational efficiency while maintaining accuracy.

Result and Discussion

Structural and Electronic Properties

The structural properties of RIn_3 and RSn_3 (R = Sm, Eu, and Gd) were determined by calculating the total energy of the unit cell as a function of volume. Bulk moduli were derived using LDA, GGA, LDA+U, and GGA+U potentials. Table 1 compares the theoretically computed results with available experimental data. The GGA-derived lattice constants for $SmSn_3$ and $GdSn_3$ exhibit closer agreement with experimental values than those obtained using GGA+U. Conversely, the GGA+U lattice constant for $EuSn_3$ aligns better with experimental data compared to GGA. This suggests that $SmSn_3$ and $GdSn_3$ exhibit itinerant behavior, while $EuSn_3$ functions as a localized compound. These results confirm that $EuSn_3$ is a divalent system, whereas $SmSn_3$ and $GdSn_3$ are trivalent. A similar trend is observed in the RIn_3 compounds. As shown in Table 1, lattice constants contract progressively from Sm to Gd, a phenomenon attributable to the lanthanide contraction. This contraction arises from the reduction in atomic radius across the lanthanide series, caused by the insufficient shielding effect of the 4f electrons. Exceptions include Eu and Yb, which exhibit divalent behavior in their 4f series (e.g., $EuIn_3$ and $EuSn_3$). Our findings corroborate these trends for both the RIn_3 and RSn_3 series. The results also reveal that LDA and LDA+U tend to underestimate lattice parameters, consistent with the general behavior of these approximations. Bulk moduli for the compounds, computed using the Birch-Murnaghan equation of state [32], are presented in Table 1. Currently, no experimental data are available for the bulk moduli or their pressure derivatives; hence, our results serve as predictions for these properties in RIn_3 and RSn_3 (R = Sm, Eu, and Gd).

TABLE 1. The calculated value of lattice parameters (a_0 in A) and bulk modulus (B_0 in GPa) of RIn_3 and RSn_3 compounds.

Compound	E_{xc}	a_0	B_0
$SmIn_3$ This work	LSDA	4.5645	60.4711
	GGA	4.6246	53.6537
	LDA +U	4.5595	56.2006
	GGA+U	4.7198	52.0019
	Exp [36]	4.626	
$EuIn_3$ This work	LSDA	4.5707	63.7229
	GGA	4.6269	53.2488
	LDA +U	4.5639	63.2119
	GGA+U	4.7592	54.2521
$GdIn_3$ This work	LSDA	4.5167	62.3367
	GGA	4.5743	66.5797
	LDA +U	4.5075	66.2844
	GGA+U	4.6557	68.5292
	Exp [36]	4.607	
$SmSn_3$ This work	LSDA	4.6052	68.8160
	GGA	4.6545	54.4352
	LDA +U	4.6135	65.4388
	GGA+U	4.7523	54.2082
	Exp [18]	4.687	

Compound	E_{xc}	a_0	B_0
$EuSn_3$ This work	LSDA	4.6313	73.2400
	GGA	4.6727	52.9966
	LDA +U	4.6316	58.2304
	GGA+U	4.7742	44.4547
	Exp [18]	4.774	
$GdSn_3$ This work	LSDA	4.6412	61.0454
	GGA	4.6412	61.0453
	LDA +U	4.5947	72.2621
	GGA+U	4.7227	67.5417
	Exp [18]	4.678	

To investigate the electronic properties of the studied compounds, we combined the total density of states (DOS) and the 4f density of states using the local density approximation (LDA) and the generalized gradient approximation (GGA). Electronic correlations are significantly pronounced in systems with 4f orbital electrons, such as lanthanides. To better understand the effects of the 4f states, we employed LDA+U, GGA+U, and incorporated spin-orbit coupling (SOC). Figs. 1–3 display the total and 4f density of states calculated using various exchange-correlation potentials for RIn_3 and RSn_3 (R = Sm, Eu, and Gd), with the Fermi level set at 0 eV.

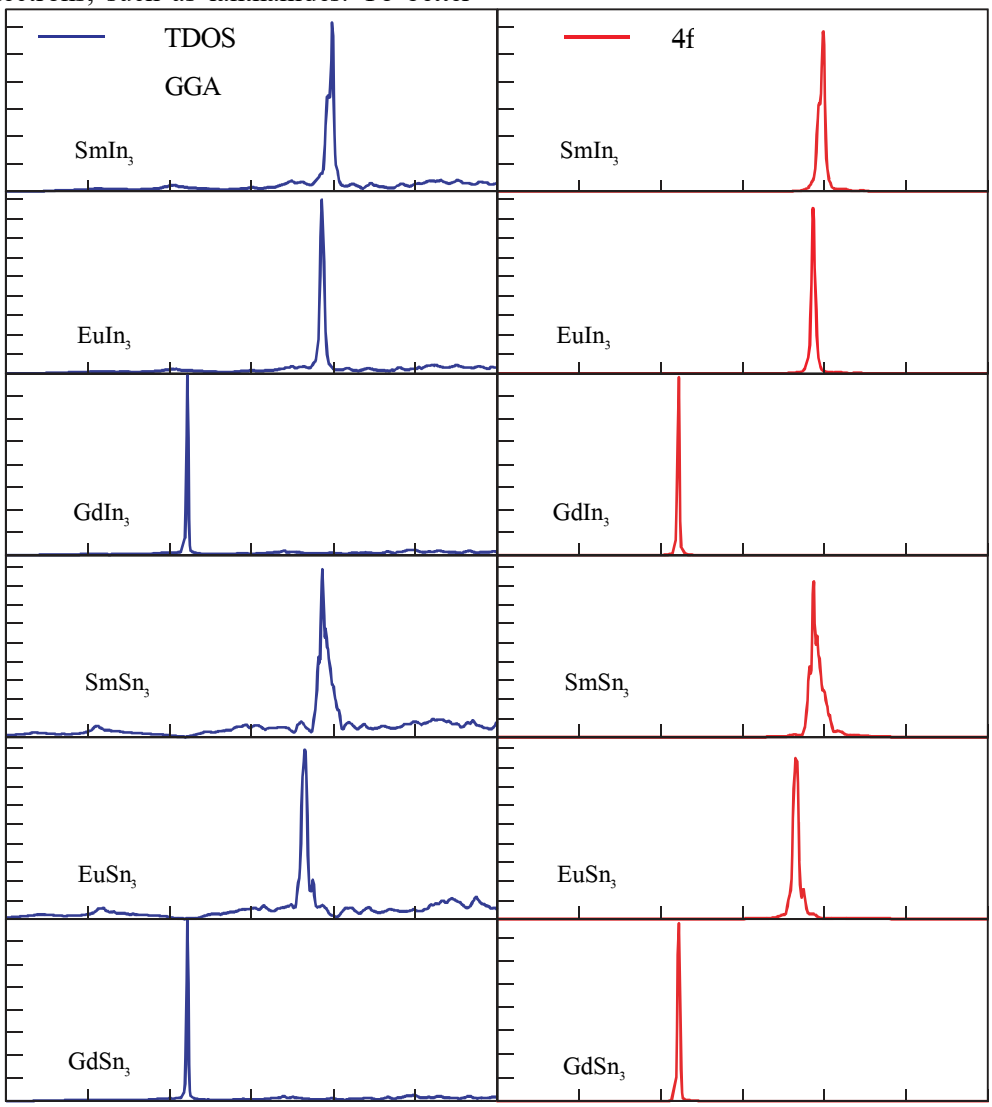

FIG. 1. Total density of states (TDOS, blue lines) and partial 4f DOS (red lines) for RIn_3 and RSn_3 (R = Sm, Eu, and Gd) calculated with GGA.

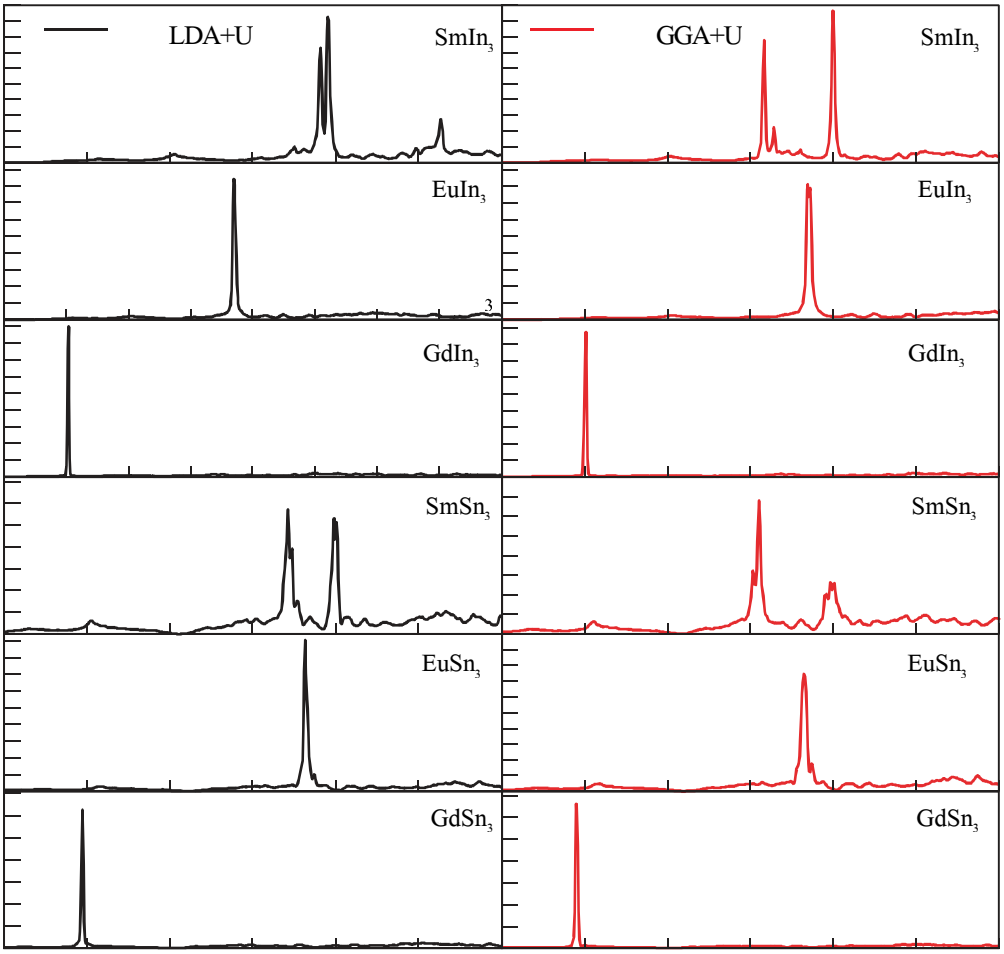

FIG. 2. Total density of states (TDOS) with LDA+U (black lines) and GGA+U (red lines) of RIn_3 and RSn_3 for R = Sm, Eu, and Gd.

Figures 1–3 reveal that no band gaps exist at the Fermi level for these intermetallic compounds, confirming their metallic nature. Figure 1 shows the total DOS (blue lines) and 4f DOS (red lines) calculated using the GGA. The dominant contribution at the Fermi level originates from the rare-earth elements. The tails of the 4f states intersect the Fermi level, except in $GdIn_3$ and $GdSn_3$, where the 4f states are positioned below the Fermi level. Peaks corresponding to 4f states are observed at specific energy levels: -0.1, -0.38, -4.5 eV ($SmIn_3$), -0.45, -0.90 eV ($EuIn_3$), and -4.5 eV ($GdIn_3$). Figure 2 presents the total and 4f DOS using the LDA+U (black lines) and GGA+U (red lines) methodologies.

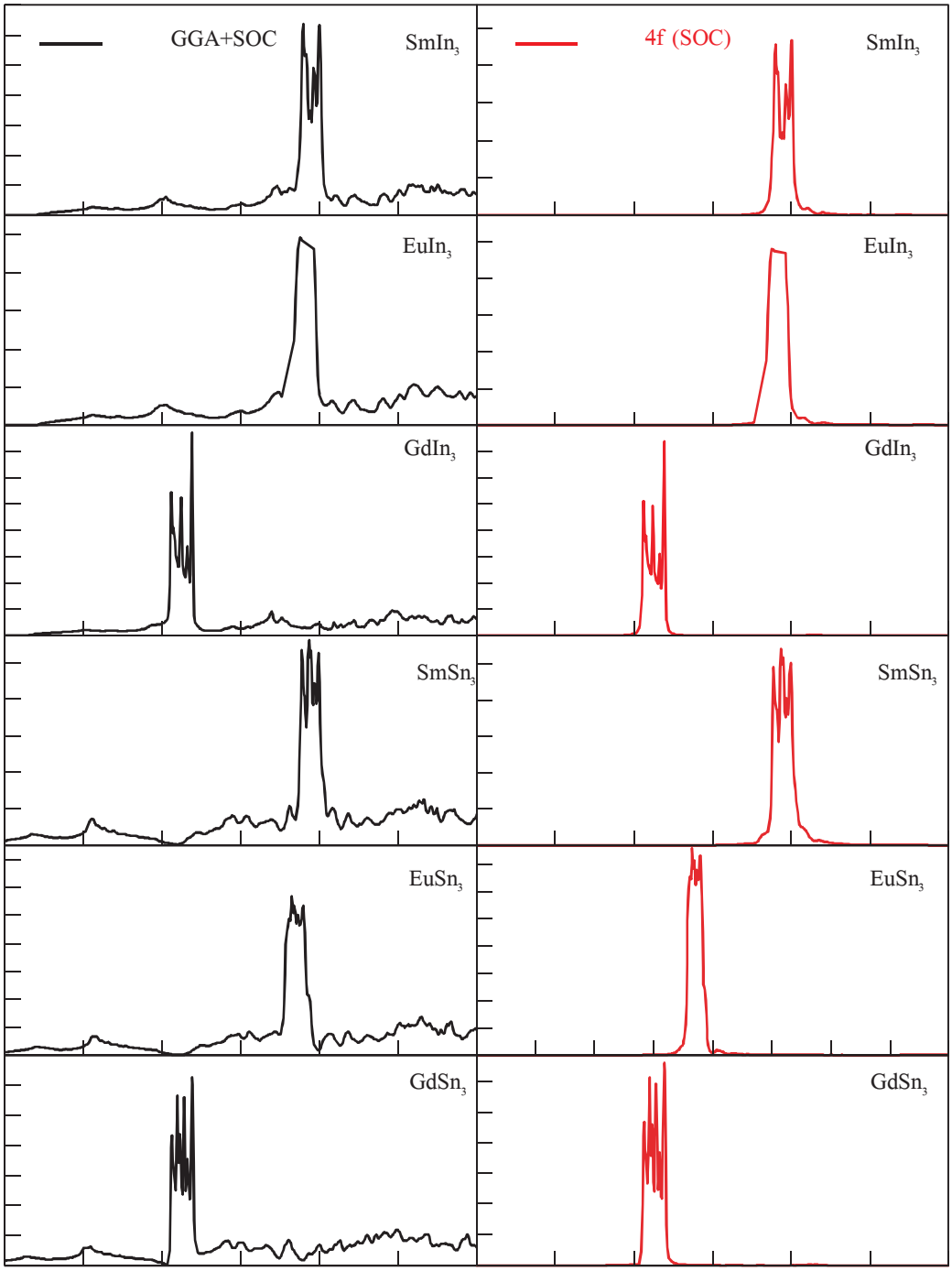

FIG. 3. Total density of states (TDOS, black lines) of RIn_3 and RSn_3 and partial 4f DOS (red lines) for R = Sm, Eu, and Gd calculated with GGA+SOC.

These results show that the inclusion of the Hubbard U parameter pushes the peaks associated with the 4f states to lower energies compared to the GGA results. This behavior is consistent with previous DFT studies, which show that the Hubbard U increases the separation between occupied and unoccupied states [33]. Figure 3 illustrates the total and 4f DOS obtained using GGA+SO. The SOC does not alter the energy positions of the 4f states but eliminates spin degeneracy, splitting the 4f DOS (determined by GGA, LDA+U, and GGA+U) into two distinct peaks. These peaks correspond to the j = 5/2 and j = 7/2 states. The j = 5/2 peaks are fully occupied in all compounds, whereas the j = 7/2 peaks are fully occupied in $GdIn_3$ and $GdSn_3$ but only partially occupied in other compounds.

Magnetic Properties

The magnetic properties of the RIn_3 and RSn_3 (R = Sm, Eu, and Gd) compounds were

investigated in terms of their magnetic moments. The RIn_3 and RSn_3 (R = Sm, Eu, and Gd) consist of the rare earth elements Sm, Eu, and Gd. Rare earth elements are renowned for their robust magnetic characteristics, rendering them a subject of interest for diverse applications such as implementation in magnetic materials and utilization as contrast agents in the field of medical imaging. The magnetic moments of these compounds would be contingent upon the computational methodology and parameters employed in the calculations. In general, magnetic moments are computed for the complete unit cell and can be further analyzed to determine the contributions from individual atoms. The magnetic moment of an atom, as used in these computations, pertains to the comprehensive magnetic moment linked to the atom within the crystal lattice. The interstitial region corresponds to the voids or gaps in the crystal structure where no atoms are present. All computed values are summarized in Table 2. The total magnetic moments of $SmIn_3$, $EuIn_3$, $GdIn_3$, $SmSn_3$, $EuSn_3$, and $GdSn_3$ compounds are dominated by the contribution of individual moments of Sm^{3+}, Eu^{3+}, and Gd^{3+}. R-4f (R=Sm, Eu, and Gd) electronic shell is responsible for the magnetic moment.

TABLE 2. Calculated spin magnetic moments (μB) of RIn_3 and RSn_3 (R = Sm, Eu, and Gd) using PBE-GGA.

	$SmIn_3$	$EuIn_3$	$GdIn_3$	$SmSn_3$	$EuSn_3$	$GdSn_3$
Interstitial region	0.02020	0.05023	0.03023	0.04129	0.01359	0.02439
R [Sm, Eu, and Gd]	6.53513	6.93514	6.63515	6.73710	6.23500	6.83974
In or Sn	-0.0370	-0.0313	-0.0119	-0.0896	-0.0245	-0.0268
Total	6.49123	6.89129	6.50127	6.67800	6.10890	6.78347

Elastic Properties

The elastic constants of a solid are crucial, as they characterize the material's response to applied stress. They are particularly relevant to various fundamental solid-state phenomena, including intraatomic bonding, equations of state, phonon spectra, and structural stability. The elastic properties are thermodynamically associated with specific heat, thermal expansion, Debye temperature, and the Gruneisen parameter. The elastic properties of solids also serve as indicators of mechanical strength, which is of considerable practical importance. Table 3 presents the calculated elastic constants C11, C12, and C44 for RIn3 and RSn3 (where R = Sm, Eu, Gd), both with and without spin polarisation, using the GGA approximation. We have compared the available experimental values of C11 and C44 for SmIn3 and SmSn3 [21]. We obtained the experimental values of C11 and C44 at 100 K and calculated the elastic constants at 0 K. Consequently, the varying temperatures result in a minor discrepancy between our calculated and experimental values. The stability of a specific crystal structure adheres to established criteria. Additionally, the computed elastic constants met the necessary stability criteria for cubic structures, specifically: C11–C12 > 0; C44 > 0; C11 + 2C12 > 0 [34, 35]. The fulfilment of the aforementioned requirements justifies the fact that these intermetallic compounds are elastically stable. Table 3 indicates that the nonmagnetic phase significantly affects the elastic characteristics of RIn_3 and RSn_3 compounds. Nonmagnetic ordering diminishes the value of the elastic constants. We derive the mechanical parameters, including bulk modulus B0, shear modulus G, Young's modulus Y, Poisson's ratio, and anisotropic ratio A, which are critical elastic parameters for industrial applications, from the elastic constants C11, C12, and C44 of the examined compounds and present them in Table 4. These are critical parameters for characterizing the mechanical properties of materials. We elucidate the mechanical properties based on the results. We define the Hill37 average shear modulus, G, as the arithmetic mean of the Voigt shear modulus, GV, and the Reuss shear modulus, GR, in terms of elastic constants.

$$G = \frac{1}{2}(G_V - G_R) \quad (1)$$

$$B = \frac{1}{2}(B_V - B_R) \quad (2)$$

where,

$$G_R = 15[4(S_{11} + S_{22} + S_{33} - S_{12} + S_{13} + S_{23}) + 3(S_{44} + S_{55} + S_{66})]^{-1} \quad (3)$$

$$G_V = \frac{1}{2}[C_{11} + C_{22} + C_{33} - (C_{12} + C_{13} + C_{23}) + 3(C_{44} + C_{55} + C_{66})] \quad (4)$$

$$B_V = \frac{1}{2}[C_{11} + C_{22} + C_{33} + 2(C_{12} + C_{13} + C_{23})] \quad (5)$$

$$B_R = [S_{11} + S_{22} + S_{33} + 2(S_{12} + S_{13} + S_{23})]^{-1} \quad (6)$$

Table 4 presents the computed values of GH, revealing that $GdSn_3$ possesses the highest GH value (44.082 GPa), while $GdIn_3$ has the lowest shear modulus value of 27.962 GPa. These two values define an interval that encompasses the remaining compounds.

TABLE 3. Calculated values of elastic constants C_{11}, C_{12}, and C_{44} (GPa) with spin polarization (GGA+SP) and without spin polarization (GGA).

Compound	E_{xc}	$SmIn_3$	$EuIn_3$	$GdIn_3$	$SmSn_3$	$EuSn_3$	$GdSn_3$
C11	GGA +SP	139.068	113.716	119.369	93.191	118.316	128.143
	GGA	100.476	100.413	118.385	99.429	94.142	114.310
	Exp. [21]	125.3			95.4		
C12	GGA +SP	60.276	56.308	63.034	42.836	61.175	59.806
	GGA	59.290	67.402	75.417	39.203	65.844	63.171
	Exp. [21]						
C44	GGA +SP	28.171	28.450	27.862	43.003	51.377	52.275
	GGA	30.426	22.588	31.348	32.211	28.788	44.195
	Exp. [21]	32.9			34.3		

Young's modulus Y, which quantifies a solid material's resistance to linear strain along its edges, is defined as the ratio of stress to strain. The compound exhibits increased stiffness with a higher value of Y. We can determine the computed values of the Voigt shear modulus G_V and the bulk modulus B_0 using the following equation:

$$Y = \frac{9BG}{3B+G} \quad (7)$$

Table 4 shows that the GdSn compound has a higher Young's modulus value compared to the other compounds. The elevated values of Young's modulus, in comparison to the bulk modulus, indicate the stiffness of these compounds.

TABLE 4. Calculated values of Voigt's shear modulus G_V, Reuss's shear modulus G_R, Hill's shear modulus G_H, B/G ratio, Cauchy pressure (C''), Poisson's ratio (v), Kleinman parameter (ξ), Anisotropy constant (A), Lames coefficient (λ and μ), and shear constant (C').

	$SmIn_3$	$EuIn_3$	$GdIn_3$	$SmSn_3$	$EuSn_3$	$GdSn_3$
G_V	32.661	28.552	27.963	35.873	42.254	45.032
G_R	31.795	28.551	27.962	33.512	38.943	43.132
G_H	32.228	28.551	27.962	34.693	40.598	44.082
Y	87.034	76.060	75.308	89.640	107.831	114.318
B/G	2.685	2.642	2.926	1.719	1.976	1.873
C''	32.105	27.858	35.208	-0.167	9.798	7.531
υ	0.332	0.332	0.347	0.249	0.276	0.269
ξ	0.728	0.826	0.879	0.769	0.861	0.780
A	0.715	0.991	0.988	1.708	1.798	1.530
λ	64.766	56.410	63.171	35.706	52.052	52.563
μ	32.661	28.552	27.963	35.873	42.254	45.032
C'	39.396	28.704	28.168	25.178	28.571	34.169

According to Pugh [34], the ratio of bulk modulus to shear modulus (B/G) can determine whether a material is ductile or brittle. We determined 1.75 as the key value that distinguishes ductile from brittle behavior. A high B/G ratio indicates ductility, while a low value signifies brittleness in materials. Table 4 clearly indicates that all compounds exhibit ductile behavior, but $SmSn_3$ is brittle. Cauchy's pressure is the disparity between two specific elastic constants (C" = C12—C44). Pittifor [35-59] suggests using Cauchy's pressure to characterize the bonding nature of the compounds under examination. The positive value of Cauchy's pressure indicates metallic bonding, whereas materials exhibiting negative Cauchy's pressure are associated with angular or directional bonding, such as covalent bonding.

An increase in the negative value of Cauchy pressure results in enhanced directional bonding and reduced mobility of the material. The calculated Cauchy's pressure for RIn_0 and RSn_0 (R = Sm, Eu, Gd) is shown in the table. All of these compounds have a positive Cauchy's pressure, which means that their bonds are metallic, except for SmSn3, which has a negative Cauchy's pressure value. The fact that $SmSn_3$ has a negative Cauchy pressure value means that it has directed or covalent bonding, which makes it brittle. Moreover, the positive and negative values of Cauchy's pressure indicate ductility and brittleness, confirming that $SmSn_3$, $EuIn_3$, $GdIn_3$, $EuSn_3$, and $GdSn_3$ are ductile, whereas $SmSn_3$ is brittle. The following formula determines the Poisson's ratio:

$$\upsilon = \frac{3B-2G}{2(3B+G)} \quad (8)$$

Poisson's ratio quantifies compressibility. As Poisson's ratio approaches 0.5, the material exhibits a tendency toward incompressibility; at v = 0.5, it is nearly incompressible. The computed values for v fall within the range of 0.25–0.5, characteristic of solids dominated by central forces. The computed values of v for the examined compounds indicate that the interatomic forces are predominantly central, with the exception of $SmSn_3$, where the central interatomic force is not prominent. Kleinman introduced a parameter known as the internal strain parameter. It delineates the comparative propensity of bond bending in relation to bond stretching. The lower limit (ξ = 0) corresponds to the minimisation of the bond bending term, while the upper limit (ξ = 1) relates to the minimisation of the bond stretching term. Subsequently, Harrison approximated the Kleinman parameter [ξ] in relation to the elastic constants using the following equation:

$$\xi = \frac{C_{11}+8C_{12}}{7C_{11}-2C_{12}} \quad (9)$$

Our computed results of ξ, which range from 0.879 to 0.728, show that bond bending predominates in our materials. However, the larger value of n suggests that bond stretching also contributes to these molecules. The elastic anisotropic ratio (A) is a crucial parameter that determines whether the elastic properties stay invariant in different directions. The following equation [33] computes the anisotropic ratio A, which directly correlates with the potential for micro-crack formation in materials:

$$A = \frac{5G_v}{G_R} + \frac{B_v}{B_R} - 6 \quad (10)$$

A equals 1 for entirely isotropic materials, and the divergence from one quantifies the degree of elastic anisotropy. The calculated values listed in Table 4 clearly suggest that these compounds are anisotropic. We can derive Lame's constants (λ, μ) from Young's modulus and Poisson's ratio using the following equation:

$$\lambda = \frac{Y\nu}{(1+\nu)(1-2\nu)}, \text{ and } \mu = \frac{Y}{2(1+\nu)} \quad (11)$$

The higher the value of Young's modulus, the greater the values of Lame's coefficients will be. The two parameters collectively form a parameterization of the elastic moduli for homogeneous isotropic media. We designate λ as Lame's first constant and μ as Lame's second constant. Values for RIn3 and RSn3 (R = Sm, Eu, Gd) are presented in Table 4. Our findings indicate that Lame's second modulus is equivalent to Voigt's shear modulus (λ = GV). For isotropic materials, λ equals C12 and μ equals C0. Our compounds exhibit high anisotropy and do not meet the criteria for isotropy, specifically $\lambda = C_{12}$ and μ = C'. We have computed the shear constant, another significant parameter, using the relation.

$$C' = \frac{1}{2}(C_{11} - C_{12}) \quad (12)$$

Table 4 presents the values for the compounds under examination. People often refer to it as the tetragonal shear modulus. Dynamical stability necessitates that $C_0 > 0$. The positive results of our computed materials show their mechanical stability. A larger shear modulus indicates more stiffness in the material against tetragonal deformation. No experimental data are available in the literature for the comparison. Subsequent experimental investigations will validate these findings. We see the current findings as a predictive analysis for these chemicals, anticipating that further experimental investigations would validate our computed results.

Conclusions

First-principles calculations were performed to theoretically investigate the structural, elastic, mechanical, and electronic properties of RIn_3 and RSn_3 (R = Sm, Eu, Gd) compounds using density functional theory (DFT). The calculated ground-state lattice parameters show excellent agreement with experimental data. The electronic density of states confirms the intermetallic nature of these compounds. Spin-orbit coupling (SOC) further splits the 4f states into two distinct peaks, modifying their energy positions.

The results demonstrate that these compounds exhibit elastic stability and anisotropy. The high values of Young's modulus indicate that certain compounds possess significant stiffness. Analysis of the B/G ratio reveals that all compounds, except $SmSn_3$, are ductile. The deviation observed in $SmSn_3$, characterized by its brittleness, suggests unique bonding characteristics that differ from those of the other compounds. Further exploration of the microstructural properties of $SmSn_3$ could provide deeper insights into the underlying mechanisms responsible for this anomaly.

Reference

[1] Tsuchida, T. and Wallace, W.E., J. Chem. Phys., 43 (1965) 3811.

[2] Buschow, K.H.J., Ferromagnetic Mater., 1 (1980) 297.

[3] Jr. Gschneidner, K.A., Russell, A., Pecharsky, A., Morris, J., Zhang, Z., Lograsso, T., Hsu, D., Lo, C.H.C., Ye, Y., Slager, A., and Kesse, D., Nature Mater., 2 (2003) 587.

[4] Jr. Gschneidner, K.A., Ji, M., Wang, C. Z., Ho, K.M., Russell, A.M., Mudryk, Y., Becker, A.T., and Larson, J.L., Acta Mater., 57 (2009) 5876.

[5] Iizuka, T., Mizuno, T., Min, B.H., Kwon, Y.S., and Kimura, S., J. Phys. Soc. Jpn., 81 (2012) 043703.

[6] Lin, C.L., Yuen, T., and Mihalisin, T., Phys. Rev. B, 54 (1996) 9254.

[7] Li, C.F., Liu, Z.Q., Shang, P.J., and Shang, J.K., Scr. Mater., 65 (2011) 1049.

[8] Asadabadi, S.J., Cottenier, S., Akbarzadeh, H., Saki, R., and Rots, M., Phys. Rev. B, 66 (2002) 195103.

[9] Bajorek, A., Chelkowska, G., Chrobak, A., and Grudziecka, M.K., Intermetallics, 26 (2012) 142.

[10] Nagai, N., Umehara, I., Ebihara, T., Albessard, A.K., Sugawara, H., Yamazaki, T., Satoh, K., and Onuki, Y., Physica B, 186 (1993) 139.

[11] Kletowski, Z., Solid State Commun., 72 (1989) 901.

[12] Buschow, K.H.J., de Wijn, H.W., and van Diephen, A.M., J. Chem. Phys., 50 (1969) 137.

[13] Percheron, A., Crorochov, O., and Achard, J.C., C. R. Acad. Sci. Paris C, 277 (1973) 81.

[14] Harris, R. and Raynor, G.V., J. Less-Common Met., 9 (1965) 7.

[15] Buschow, K.H.J., Phys. Lett. A, 29 (1969) 12.

[16] Gorlich, E., Hrynkiewicz, H., Kmied, R., Catka, K., Tomala, K., Czopnik, A., and Iliew, N., Phys. Status Solidi A, 30 (1975) K17.

[17] Buschow, K.H.J., Rep. Prog. Phys., 42 (1979) 1373.

[18] Sanchez, J.P., Friedt, J.M., Shenoy, G.K., Percheron, A., and Achard, J.C., J. Phys. C: Solid State Phys., 9 (1976) 2207.

[19] Onuki, Y. and Settai, R., Low Temp. Phys., 38 (2012) 89.

[20] Asadabadi, S.J. and Akbarzadeh, H., Physica B, 349 (2004) 76.

[21] Endoh, D., Goto, T., Tamaki, A., Liu, B., Kasaya, M., Fujimura, T., and Kasuya, T., J. Phys. Soc. Jpn., 58 (1989) 940.

[22] Suna, Z., Lib, S., Ahuja, R., and Schneidera, J.M., Solid State Commun., 129 (2004) 589.

[23] Blaha, P., Schwarz, K., Madsen, G.K.H., Kuasnicka, D., and Luitz, J., "WIEN2K, An Augmented Plane WaveþLocal Orbitals Program for Calculating Crystal Properties", edited by K. Schwarz, (Technical Universitat, Wien, Austria, 2001).

[24] Andersen, O.K., Phys. Rev. B, 12 (1975) 3060.

[25] Perdew, J.P. and Zuanger, A., Phys. Rev. B, 23 (1981) 5048.

[26] Perdew, J.P., Burke, K., and Ernzerhop, M., Phys. Rev. Lett., 77 (1996) 3865.

[27] Anisimov, V.I., Solovyev, I.V., Korotin, M.A., Czyzyk, M.T., and Sawatzky, G.A., Phys. Rev. B, 48 (1993) 16929.

[28] Monkhorst, H.J. and Pack, J.D., Phys. Rev. B, 13 (1976) 5188.

[29] Jamal, M., Cubic-elastic, http://www.wien2k.at/ reg_user/unsupported/ (2012).

[30] Jamal, M. and Jalali, S., Asadabadi, e-print arXiv:submit/0630082 [cond-mat.mtrl-sci] (2013).

[31] Stadler, R., Wolf, W., Podloucky, R., Kresse, G., Furthmuller, J., and Hafner, J., Phys. Rev. B, 54 (1996) 1729.

[32] Birch, F., Phys. Rev., 71 (1947) 809.

[33] Hill, R., Proc. Phys. Soc. London, 65 (1952) 349.

[34] Pugh, S. F., Philos. Mag., 45 (1954) 823.

[35] Pettifor, D.G., Mater. Sci. Technol., 8 (1992) 345.

[36] Schwartz, G.P. and Shirley, D.A., Hyperfine Interact., 3 (1977) 67.

[37] Gautam, R., Kumar, A., and Singh, R., Acta Phys. Pol. A, 132 (4) (2017) 1371.

[38] Kumar, A., Gautam, R., Chand, S., Kumar, A., and Singh, R.P., Mater. Phys. Mech., 42 (1) (2019) 112.

[39] Kumar, A., Gautam, R., Singh, R.P., and Kumar, A., Int. J. Adv. Sci. Technol., 29 (08) (2020) 1150.

[40] Annveer, Gautam, R., Kumar, A., Kumar, A., Singh, P.K., and Singh, R.P., Optik, 223 (2020) 165317.

[41] Annveer, Gautam, R., Kumar, A., Kumar, A., Gautam, Y.K., Saroj, A.L., and Singh, R.P., J. Mater. Sci.: Mater Electron, 32 (2021) 727.

[42] Kumar, A., Kumar, A., Kumar, K., Singh, R.P., Singh, R., and Kumar, R., East Eur. J. Phys., 1 (2023) 109.

[43] Kumar, A., Singh, N.K., Israil, M., Gupta, E., Singh, N., and Sharma, A.K., Subharti J. Interdiscip. Res., 6 (1) (2023) 1.

[44] Narayan, Y., Kumar, A., Singh, A.P., Ahsan, M., Upadhayay, R.K., and Rao, L.M., Eur. Chem. Bull., 12 (2023) 494.

[45] Veerta, Kumar, A., and Kumar, A., Int. Res. J. Manag. Sci. Technol., 14 (2023) 176.

[46] Lal, B., Kumar, A., and Kumar, A., Int. J. Res. Anal. Rev., 10 (2) (2023) 952.

[47] Kumar, A., Kumari, K., and Sharma, S.K., Twist, 19 (2024) 275.

[48] Singh, N.K., Kumar, A., and Kiran, A., Twist, 19 (2024) 338.

[49] Kumar, A., Gupta, H., Kumar, D., Sharma, R., Kumar, A., Sharma, S.K., and Singh, A.P., East Eur. J. Phys., 1 (2024) 355.

[50] Kumar, A., Kumar, A., Pundir, S.K., and Singh, N., Twist, 19 (2024) 377.

[51] Kumar, A., Singh, M., and Kumar, R., Twist, 19 (2024) 439.

[52] Kumar, A., Kumar, A., Kumar, A., and Iram, N., Hybrid Adv., 6 (2024) 100197.

[53] Kumar, A., Kumar, A., and Iram, N., Hybrid Adv., 6 (2024) 100211.

[54] Kumar, A., Gupta, H., Kumar, A., Kumar, A., Sharma, S.K., Lal, B., and Iram, N., Indian J. Phys., (2024), https://doi.org/ 10.1007/s12648-024-03273-6.

[55] Kumar, A., Kumar, A., Jain, P., Pundir, S.K., and Singh, N., Optik, 315 (2024) 172039.

[56] Kumar, A., Kumar, S., Pundir, S.K., Nautiyal, V.K., Kumar, A., and Iram, N., Opt. Quantum Electron., 56 (2024) 1742.

[57] Kumar, A., Kumar, R., Kumar, R., and Kumar, A., Mater. Phys. Mech., 52 (4) (2024) 23.

[58] Peng, Q., Iram, N., Sharma, R., Kumar, A., Alsubaie, A.S., and Rehman, J., Inorg. Chem. Commun., 170 (1) (2024) 113240.

[59] Iram, N., Sharma, R., Ahmad, J., Kumar, A., Kumar, A., Almutairi, F.N., and Alturaifi, H.A., Inorg. Chem. Commun., 172 (2024) 113573.